

# 1 The pH dependency of the boron isotopic composition of diatom opal 2 (*Thalassiosira weissflogii*)

3 Hannah K. Donald<sup>1</sup>, Gavin L. Foster<sup>1,\*</sup>, Nico Fröhberg<sup>1</sup>, George E. A. Swann<sup>2</sup>, Alex J. Poulton<sup>3,4</sup>, C. Mark  
4 Moore<sup>1</sup> and Matthew P. Humphreys<sup>5</sup>

5

6 <sup>1</sup>School of Ocean and Earth Science, National Oceanography Centre Southampton, University of  
7 Southampton, Southampton, SO14 3ZH

8 <sup>2</sup>School of Geography, University of Nottingham, University Park, Nottingham, NG7 2RD

9 <sup>3</sup>Ocean Biogeochemistry and Ecosystems, National Oceanography Centre, Southampton, SO14 3ZH

10 <sup>4</sup>The Lyell Centre, , Heriot-Watt University, Edinburgh, EH14 4AS

11 <sup>5</sup>NIOZ Royal Netherlands Institute for Sea Research, Department of Ocean Systems (OCS), and Utrecht  
12 University, PO Box 59, 1790 AB Den Burg (Texel), the Netherlands

13 \*Corresponding Author

14

## 15 **Abstract**

16 The high latitude oceans are key areas of carbon and heat exchange between the atmosphere and the  
17 ocean. As such, they are a focus of both modern oceanographic and palaeoclimate research. However,  
18 most palaeoclimate proxies that could provide a long-term perspective are based on calcareous  
19 organisms, such as foraminifera, that are scarce or entirely absent in deep-sea sediments south of  
20 50°S in the Southern Ocean and north of 40°N in the North Pacific. As a result, proxies need to be  
21 developed for the opal-based organisms (*e.g.* diatoms) found at these high latitudes, which dominate  
22 the biogenic sediments recovered from these regions. Here we present a method for the analysis of  
23 the boron (B) content and isotopic composition ( $\delta^{11}\text{B}$ ) of diatom opal. We apply it for the first time to  
24 evaluate the relationship between seawater pH,  $\delta^{11}\text{B}$  and B concentration ([B]) in the frustules of the  
25 diatom *Thalassiosira weissflogii*, cultured across a range of carbon dioxide partial pressure ( $p\text{CO}_2$ ) and  
26 pH values. In agreement with existing data, we find that the [B] of the cultured diatom frustules  
27 increases with increasing pH (Mejia et al., 2013).  $\delta^{11}\text{B}$  shows a relatively well-defined negative trend  
28 with increasing pH, completely distinct from any other biomineral previously measured. This  
29 relationship not only has implications for the magnitude of the isotopic fractionation that occurs  
30 during boron incorporation into opal, but also allows us to explore the potential of the boron-based  
31 proxies for palaeo-pH and palaeo- $\text{CO}_2$  reconstruction in high latitude marine sediments that have, up  
32 until now, eluded study due to the lack of suitable carbonate material.

33

## 34 **1. Introduction**

35 The high latitude regions, such as the Southern Ocean and the subarctic North Pacific Ocean, exert  
36 key controls on atmospheric carbon dioxide ( $\text{CO}_2$ ) content. Both areas are where upwelling of deep  
37 carbon- and nutrient-rich water occurs, which promotes outgassing of previously stored carbon to the  
38 atmosphere and nutrient fertilisation of primary productivity, in turn drawing down  $\text{CO}_2$ . The balance  
39 of processes involved in determining whether these oceanic regions are a source or sink of  $\text{CO}_2$  are  
40 poorly understood, to the extent that the oceanic controls on glacial-interglacial pH and  $p\text{CO}_2$  changes

41 remain a subject of vigorous debate (*e.g.* Martin, 1990; Sigman and Boyle, 2000). Recently, several  
42 studies have shown how the boron isotope pH proxy applied to calcitic foraminifera successfully tracks  
43 surface water CO<sub>2</sub> content, thus documenting changes in air-sea CO<sub>2</sub> flux along the margins of these  
44 regions (*e.g.* Martínez-Botí et al., 2015; Gray et al. 2018). However, the lack of preserved marine  
45 carbonates in areas that are thought to be key in terms of glacial-interglacial CO<sub>2</sub> change (*e.g.* the  
46 polar Antarctic zone; Sigman et al., 2010) represents a currently insurmountable problem, preventing  
47 the determination of air-sea CO<sub>2</sub> flux using boron-based proxies in regions that are likely to play the  
48 most important role in glacial-interglacial CO<sub>2</sub> change. There is therefore a clear need for the boron  
49 isotope palaeo-pH proxy to be developed in biogenic silica (diatom frustules, radiolarian shells), which  
50 is preserved in high-latitude settings, to better understand these key regions and their role in natural  
51 climate change.

52

53 The boron isotopic system has been used extensively in marine carbonates for the reconstruction of  
54 past ocean pH and past atmospheric *p*CO<sub>2</sub> (*e.g.* Hemming and Hanson, 1992; Pearson and Palmer,  
55 2000; Hönisch and Hemming, 2005; Foster, 2008; Henehan et al., 2013; Chalk et al. 2017; Sosdian et  
56 al. 2018). Comprehensive calibration work has been completed for numerous species of foraminifera  
57 that are currently used in palaeoceanographic reconstruction (*e.g.* Henehan et al. 2016; Rae et al.  
58 2011). From this it has been shown that while  $\delta^{11}\text{B}$  compositions are fairly similar among carbonates,  
59 species-specific differences exist in the relationship between the  $\delta^{11}\text{B}$  of dissolved borate and that of  
60 foraminifera. Once this relationship is known, this  $\delta^{11}\text{B}$ -pH calibration can be applied to fossils found  
61 in deep-sea sediment cores, reliably reconstructing past ocean pH and *p*CO<sub>2</sub> (*e.g.* Hönisch and  
62 Hemming, 2005; Foster, 2008, Hönisch et al., 2009; Chalk et al., 2017). However, thus far the boron  
63 isotopic composition (expressed as  $\delta^{11}\text{B}$ ) and B concentration ([B]) of the siliceous fraction of deep-  
64 sea sediments remains poorly studied.

65

66 Early exploratory work by Ishikawa and Nakamura (1993) showed that biogenic silica and diatom ooze  
67 collected from modern deep-sea sediments in the North and Equatorial Pacific had relatively high  
68 boron contents (70-80 ppm), but a very light isotope ratio. For example, a diatom ooze was shown to  
69 have a  $\delta^{11}\text{B}$  of -1.1 ‰ whilst radiolarian shells had a  $\delta^{11}\text{B}$  of +4.5 ‰. While some of this light  $\delta^{11}\text{B}$  may  
70 have partly arisen due to clay contamination (reducing the diatom ooze sample by up to 3 ‰; Ishikawa  
71 and Nakamura, 1993) it also likely reflects an opal:seawater isotopic fractionation arising from the  
72 substitution of borate for silicate in tetrahedral sites in the opal (Ishikawa and Nakamura, 1993). A  
73 similarly light  $\delta^{11}\text{B}$  was also observed in marine cherts from deep sea sediments by Kolodny and  
74 Chaussidon (2004; -9.3 to +8 ‰), but these are likely diagenetic and therefore unlikely to be primary

75 seawater precipitates. A recent culture study of the diatoms *Thalassiosira weissflogii* and *T.*  
76 *pseudonana* showed that the boron content of cultured opal was significantly lower than suggested  
77 by the bulk sampling of Ishikawa and Nakamura (1993) at around 5-10 ppm, increasing as pH increased  
78 from 7.6 to 8.7 (Mejia et al., 2013). This suggests seawater tetrahydroxyborate anion (borate;  $B(OH)_4^-$ )  
79 is predominantly incorporated into the diatom frustule rather than boric acid ( $B(OH)_3$ ) and implies  
80 there is potential for the boron content of diatom opal to trace pH in the past (Mejia et al., 2013).

81

82 Here, the relationship between  $\delta^{11}B$  of the frustules of the diatom *T. weissflogii* and seawater pH is  
83 investigated for the first time using a batch culturing technique and different air-CO<sub>2</sub> mixtures to  
84 explore a range of pH ( $8.54 \pm 0.57$  to  $7.48 \pm 0.06$ ). The aim of this study was also to develop a  
85 methodology for measuring the boron isotopic composition of biogenic silica by MC-ICP-MS and apply  
86 this method to explore the response of the boron-based proxies ([B] and  $\delta^{11}B$ ) in diatom frustules to  
87 changing pH. Ultimately, we show how boron isotopes measured in diatom frustules may provide  
88 further insight into boron uptake and physiological activity within diatoms and test the potential of  
89  $\delta^{11}B$  and boron content in diatoms as proxies for the ocean carbonate system.

90

## 91 **2. Methods**

### 92 **2.1 Experimental Set up**

93 The centric diatom *T. weissflogii* (Grunow in van Heurck, PCC 541, CCAP 1085/1; Hasle and Fryxell,  
94 1977) was grown in triplicate in enriched sterile and filtered seawater (K/1; 0.2  $\mu m$ ; seawater sourced  
95 from Labrador Sea; Keller et al., 1987) in 3 L glass Erlenmeyer flasks for a maximum of one week for  
96 each experiment. Initial nutrient concentrations within the seawater before enrichment were  
97 assessed on a SEAL Analytical QuAAtro analyser with a UV/vis spectrometer and ranged from 23.3 to  
98 27.5  $\mu M$  for nitrate(+nitrite), 4.3 to 5.4  $\mu M$  for silicic acid and 1.4 to 1.6  $\mu M$  for phosphate. The culture  
99 experiments were bubbled with air-CO<sub>2</sub> mixtures in different concentrations (sourced from BOC ; ;  
100 [www.boconline.co.uk](http://www.boconline.co.uk)) to provide a pH range at constant bubble rates, and every flask was agitated  
101 by hand twice daily to limit algal settling and aggregation. The monocultures were grown in nutrient  
102 replete conditions at constant temperature (20°C) and on a 12h:12 h light:dark cycle (with 192  $\mu E m^{-2}$   
103  $s^{-1}$ , or 8.3  $E m^{-2} d^{-1}$  during the photoperiod). The diatoms were acclimated to each  $pCO_2$  treatment for  
104 at least 10 generations before inoculating the culture experiment flasks. All culture handling was  
105 completed within a laminar flow hood to ensure sterility. The flow hood surfaces were cleaned with  
106 90% ethanol before and after handling, as well as the outer surface of all autoclaved labware entering  
107 the laminar flow hood such as bottles and pipettes.

108

109 The cultured diatom samples were collected by centrifugation at 96 h, during the exponential growth  
110 phase. Each flask was simultaneously disconnected from the gas supply with the culture immediately  
111 centrifuged at 3700 rpm for 30 minutes into a pellet, rinsed with MilliQ, and frozen at -20°C in sterile  
112 plastic 50 mL centrifuge tubes. Around 10 mg of diatom biomass was harvested in each experiment.

113

## 114 **2.2. Growth rate and cell size**

115 A 5 mL sub-sample was taken from each culture flask through sterilised Nalgene tubing into sterile  
116 syringes and sealed in sterile 15 mL centrifuge tubes. Triplicate cell counts using a Coulter  
117 Multizier<sup>TM3</sup> (Beckman Coulter) were performed daily on each experimental flask. Growth rates were  
118 calculated using equation 1:

$$119 \quad \mu = (\ln N_t - \ln N_i) / (t - t_i) \quad (1)$$

120 where  $N_i$  is the initial cell density at the start of the experiment ( $t_i$ ) and  $N_t$  is the cell density at time  $t$ .

121 Triplicate estimates of cell size were also determined using the Coulter Multizier<sup>TM3</sup>, to determine  
122 the mean cell size over time in each flask. Figure 1 shows that although there is no statistically  
123 significant relationship between pH and diatom growth rate, cell size does show a small, but  
124 statistically significant, positive slope.

## 125 **2.3 pH, DIC and $\delta^{11}\text{B}$ of the culture media**

126 A pH meter (Orion 410A) calibrated using standard National Bureau of Standards (NBS) buffers prior  
127 to sample extraction was used to monitor the evolution of pH through the experiment on a daily  
128 basis. For fully quantitative constraints on the carbonate system of the culture media, dissolved  
129 inorganic carbon (DIC) was measured in triplicate, every other day, for each pH treatment (*i.e.* once  
130 per experiment flask). The 100 mL sample bottles were filled to overflowing and immediately closed  
131 with ground glass stoppers, then uncapped to be poisoned with 20  $\mu\text{L}$  saturated mercuric chloride  
132 solution ( $\text{HgCl}_2$ ) to prevent any further biologically-induced changes in DIC, before being sealed with  
133 a 1 mL air headspace and Apiezon L grease, and stored in complete darkness until analysis (Dickson  
134 et al., 2007). Analysis of DIC was performed by acidification with excess 10% phosphoric acid and  $\text{CO}_2$   
135 transfer in a nitrogen gas stream to an infrared detector using a DIC Analyzer AS-C3 (Apollo SciTech,  
136 DE, USA) at the University of Southampton. The DIC results were calibrated using measurements of  
137 batch 151 certified reference material obtained from A. G. Dickson (Scripps Institution of  
138 Oceanography, CA, USA). The accuracy of the DIC analysis was ca. 3  $\mu\text{mol kg}^{-1}$ . Carbonate system  
139 parameters, including seawater  $\text{pCO}_2$ , were calculated using measured  $\text{pH}_{\text{NBS}}$  and DIC values,

140 temperature, salinity and nutrients with the CO<sub>2</sub>SYS v1.1 program (van Heuven et al., 2011; using  
141 constants from Dickson, 1990; Lueker et al., 2000; Lee et al., 2010), which was also used to convert  
142 pH meter readings from the NBS to the Total scale (used throughout).

143 All flasks were initially filled with media from the same large batch and all culture treatments  
144 therefore started with the same initial pH. The pH for all treatments was then altered by bubbling  
145 through the different air-CO<sub>2</sub> mixtures, ranging from low pH (target = 1600 ppm, high *p*CO<sub>2</sub>) to high  
146 pH (target = 200 ppm, low *p*CO<sub>2</sub>). Almost all treatments held relatively constant DIC and pH until the  
147 final 24 hours of the experiment, when marked changes in DIC and pH in all culture treatments were  
148 observed (Figure 2), which in most cases was likely due to the growth of diatoms and an associated  
149 net removal of DIC, despite the constant addition of *p*CO<sub>2</sub>. In order to account for these non-steady  
150 state conditions of the carbonate system, the mean pH and *p*CO<sub>2</sub> of each treatment were calculated  
151 based on the number of cells grown per 24 hours along with the pH/*p*CO<sub>2</sub> measured in that 24 hours,  
152 thus adjusting for the observed exponential growth rate of *T. weissflogii* (Table 1).

153

154 The boron concentration of the culture media was not determined but is assumed to be the same as  
155 Labrador seawater (~4.5 ppm; Lee et al., 2010). The boron isotopic composition of the culture media  
156 was determined using standard approaches (Foster et al., 2010) to be 38.8 ± 0.19 ‰ (2 s.d.).

#### 157 **2.4 Preparing cultured diatoms for δ<sup>11</sup>B and B/Si analysis**

158 In order to examine reproducibility and accuracy of our boron measurements, an in-house diatom  
159 reference material was used to develop a method for measuring boron isotopes and boron  
160 concentration in biogenic silica. A British Antarctic Survey core catcher sample (TC460) from core  
161 TC460 in the Southern Ocean (-60.81534° N, -50.9851° E, water depth 2594 m) was used for this  
162 purpose (supplied by C.-D. Hildebrand [British Antarctic Survey]). Although the diatom assemblage  
163 was not characterised in the core catcher, the nearest sediment sample in the core is dominated by  
164 *Hyalochaete Chaetoceros* resting spores, representing circa 70% of the total diatom content, with sea  
165 ice and cool open water species making up the bulk of the remaining 30% (e.g. *Actinocyclus*  
166 *actinochilus*, *Fragilariopsis curta*, *F. cylindrus*, *F. obliquecostata*, *Odontella weissflogii*, *Thalassiosira*  
167 *antarctica*). A pure diatom sample of mixed species was separated from this bulk sediment and  
168 cleaned of clay contamination at the University of Nottingham following an established diatom  
169 separation technique (Swann et al., 2013). Briefly, the bulk sample underwent organic removal and  
170 carbonate dissolution (using 30% H<sub>2</sub>O<sub>2</sub> and 5% HCl), heavy liquid separation in several steps at  
171 different specific gravities using sodium polytungstate (SPT) and visual monitoring throughout the  
172 process to ensure the sample was free from non-diatom material, such as clay particulates. After the

173 final SPT separation, samples were rinsed thoroughly with MilliQ and sieved at 10  $\mu\text{m}$  to remove all  
174 SPT traces.

175

176 The culture samples and the diatom fraction from TC460 were first acidified ( $\text{H}_2\text{SO}_4$ ) and organics were  
177 oxidised using potassium permanganate and oxalic acid (following Horn et al., 2011 and Mejía et al.,  
178 2013). The samples were rinsed thoroughly using MilliQ water via centrifugation and transferred to  
179 acid-cleaned Teflon beakers. A secondary oxidation was completed under heat using perchloric acid.  
180 Finally, the organic-free samples were rinsed thoroughly with MilliQ via filtration.

181

182 In the boron-free HEPA filtered clean laboratory at the University of Southampton, each sample was  
183 dissolved completely in a gravimetrically known amount of NaOH (0.5 M from 10 M concentrated  
184 stock supplied by Fluka) at 140°C for 6 to 12 h and briefly centrifuged prior to boron separation to  
185 ensure no insoluble particles were loaded onto the boron column. Anion exchange columns containing  
186 Amberlite IRA 743 resin were then used to separate the matrix from the boron fraction of each sample  
187 following Foster (2008). Briefly, the dissolved opal was loaded directly onto the column without  
188 buffering and the matrix removed with 9 x 200  $\mu\text{L}$  washes of MilliQ. This was collected for subsequent  
189 analysis and the pure boron fraction was then eluted and collected in 550  $\mu\text{L}$  of 0.5 M  $\text{HNO}_3$  acid. The  
190 level of potential contamination was frequently monitored using total procedural blanks (TPB)  
191 measured in every batch of columns. The TPB comprised an equivalent volume of sodium hydroxide  
192 (NaOH, 0.5 M) as used in the samples of each batch (ca. 0.2 - 4 mL). This was analysed following the  
193 sample analysis protocols detailed below, typically the TPBs for this work contained less than 40 pg of  
194 boron. This equates to a typical blank contribution of ca. 0.015%, which results in a negligible  
195 correction and is therefore ignored here.

196

197 Prior to isotope analysis, all boron fractions were collected in pre-weighed acid cleaned Teflon beakers  
198 and their mass was recorded using a Precisa balance. A 10  $\mu\text{L}$  aliquot was taken and diluted with 490  
199  $\mu\text{L}$  0.5 M  $\text{HNO}_3$  in acid cleaned plastic centrifuge tubes (2 mL). This was then analysed using a Thermo  
200 Fisher Scientific Element 2XR ICP-MS at the University of Southampton, with boron concentration  
201 determined using standard approaches and a gravimetric standard containing boron, silicon, sodium  
202 and aluminium. In order to determine the B/Si ratio and hence the B concentration of the opal, the Si  
203 concentration must also be quantitatively measured. This is achieved here by using a known  
204 concentration and mass of NaOH to dissolve each sample, by measuring the Si/Na ratio the Si  
205 concentration of each opal sample can be determined. From this, assuming a chemical formula of  
206  $\text{SiO}_2 \cdot \text{H}_2\text{O}$  and a  $\text{H}_2\text{O}$  content of 8% (Hendry and Anderson, 2013), the B content of the opal in ppm can

207 be estimated. As detailed above, during the purification procedure, sample matrix was washed off the  
208 column using MilliQ and collected in pre-weighed acid cleaned Teflon beakers. These samples were  
209 then diluted with 3 % HNO<sub>3</sub> enriched with Be, In and Re for the internal standardisation and measured  
210 on the Thermo Scientific X-series ICP-MS. The standards run on the X-Series consisted of varied  
211 concentrations of the gravimetric standard also used on the Element, containing B, Si, Na and Al.

212

213 The boron isotopic composition of the biogenic silica samples was determined on a Thermo Scientific  
214 Neptune MC-ICP-MS, also situated in a boron-free HEPA filtered laboratory at the University of  
215 Southampton, following Foster (2008). Instrument induced fractionation of the <sup>11</sup>B/<sup>10</sup>B ratio was  
216 corrected using a sample-standard bracketing routine with NIST SRM 951, following Foster (2008).  
217 This allows a direct determination of δ<sup>11</sup>B without recourse to an absolute value for NIST SRM 951  
218 (Foster, 2008) using the following equation, where <sup>11</sup>B/<sup>10</sup>B<sub>standard</sub> is the mean <sup>11</sup>B/<sup>10</sup>B ratio of the  
219 standards bracketing the sample of interest.

220

$$221 \quad \delta^{11}\text{B} = \left[ \left( \frac{{}^{11}\text{B}/{}^{10}\text{B}_{\text{sample}}}{{}^{11}\text{B}/{}^{10}\text{B}_{\text{standard}}} \right) - 1 \right] \times 1000 \quad (2)$$

222

223 The reported δ<sup>11</sup>B is an average of the two analyses, with each representing a fully independent  
224 measurement (*i.e.* the two measurements did not share blanks or bracketing standards). Machine  
225 stability and accuracy was monitored throughout the analytical session using repeats of NIST SRM 951,  
226 as well as boric acid reference materials AE120, AE121 and AE122 that gave δ<sup>11</sup>B (± 2 s.d.) of -20.19 ±  
227 0.20 ‰, 19.60 ± 0.28 ‰, and 39.31 ± 0.28 ‰, that are within error of the gravimetric values from Vogl  
228 and Rosner (2012).

229

230 The reproducibilities of the δ<sup>11</sup>B and [B] measurements were assessed by repeat measurements of  
231 TC460 of different total B concentration (11 to 34 ng of B). In order to assess the accuracy of this  
232 method, we follow Tipper et al. (2008) and Ni et al. (2010) and use standard addition. To this end,  
233 known amounts of NIST SRM 951 standard were mixed with known quantities of TC460. All mixtures  
234 were passed through the entire separation and analytical procedure, including aliquots of pure  
235 standard and sample. A sodium acetate - acetic acid buffer was added to all 951 boric acid used prior  
236 to mixing, to ensure the pH was sufficiently elevated for the column separation procedure (following  
237 Foster, 2008). The amount of biogenic silica matrix added to the columns for each mixture was kept  
238 constant, so the volume added to the column was altered for each mixture accordingly. Uncertainty  
239 in the δ<sup>11</sup>B calculated for each mixture was determined using a Monte Carlo procedure (n = 1000) in

240 R (R Core Team, 2019) propagating uncertainties, at 95% confidence, in known isotopes ratios ( $\pm 0.2$   
241 ‰), sample concentration ( $\pm 6\%$ ) and measured masses ( $\pm 0.5\%$ ).

242

### 243 **3. Results and Discussion**

#### 244 **3.1 Analytical Technique**

##### 245 **3.1.1. Purification**

246 The Na, Si, and Al concentrations of the matrix fraction of several replicates of the diatom fraction of  
247 TC460 are shown in Figure 3a-d. Prior to purification, Na and Si concentrations were consistently  
248 around 265 and 114 ppm respectively, whereas Al was more variable at 5-25 ppb. The boron content  
249 of these matrix samples in all cases was at blank level. The concentration of these elements in the  
250 boron fraction is shown in Figure 3e-g, highlighting that the column procedure was sufficient to  
251 concentrate boron and remove Na and Si, which are both present at sub-5 ppb level (*i.e.* at less than  
252 0.002 ‰ of matrix concentration). The Al is likely present in the diatom frustule (*e.g.* Koning et al.,  
253 2007) and is elevated in the boron fraction compared to the matrix fraction (Figure 3). Diatom-bound  
254 Al is likely present as the anion  $\text{Al}(\text{OH})_4^-$ , hence its elevation in the boron fraction. Although this is a  
255 detectable level of Al, it is unlikely that this level of contamination will influence the mass fractionation  
256 of these samples when measured by MC-ICP-MS (Foster, 2008; Guerrot et al., 2010).

257

##### 258 **3.1.2. Accuracy and Reproducibility**

259 Throughout the duration of this study, a single dissolution of the diatom fraction of TC460 was  
260 measured 18 times in separate analyses at various concentrations, in order to assess external  
261 reproducibility of this method. Carbonates generally have a reproducibility of  $\pm 0.20\%$  ( $2\sigma$ ) at an  
262 analyte concentration of 50 ppb boron using the MC-ICP-MS methods at the University of  
263 Southampton (*e.g.* Chalk et al., 2017). The repeated measurements of TC460 gave a reproducibility of  
264  $\pm 0.28\%$  ( $2\sigma$ ) over 18 samples, ranging from 19 ppb to 61 ppb (11 to 34 ng) boron (Figure 4). The  
265 insensitivity of  $\delta^{11}\text{B}$  to the boron concentration analysed confirms that blank contamination during  
266 purification is not significant. Figure 4 shows that there is also no correlation between Al content of  
267 the boron fraction and measured  $\delta^{11}\text{B}$ , confirming that Al contamination does not influence mass  
268 fractionation.

269

270 Figure 4 shows the results of the standard addition experiment, and when the uncertainty in the  $\delta^{11}\text{B}$   
271 of the mixture is considered, it is clear that nearly all the mixtures lie within error of the 1:1 line,  
272 indicating that there is a lack of a significant matrix effect when analysing the  $\delta^{11}\text{B}$  of biogenic silica as  
273 described herein. A least-squares linear regression of the mixtures has a slope of  $1.01 \pm 0.07$  and an



274 intercept of  $-0.15 \pm 0.29 \text{ ‰}$ , implying the approach is accurate to  $\pm 0.29 \text{ ‰}$ , which is remarkably similar  
275 to the stated reproducibility of TC460 ( $\pm 0.28 \text{ ‰}$  at  $2\sigma$ ).

276

277 B and Si content were determined separately and combined post-analysis in order to estimate the  
278 B/Si ratio for each sample and hence the B concentration. The reproducibility of this method was  
279 tested using six repeats of the diatom fraction of TC460. The mean of all six measurements is  $2.99 \pm$   
280  $0.64 \text{ ppm}$ ; ( $2\sigma$ ; Figure 4), implying this multi-stage method of determining the B content of diatoms is  
281 precise to  $\pm 20 \%$  at 95% confidence.

282

### 283 **3.2. Diatom Cultures**

#### 284 **3.2.1. Boron content of the frustule of *T. weissflogii***

285 The boron content of *T. weissflogii* increases as a function of pH from around  $\sim 1 \text{ ppm}$  to  $\sim 4 \text{ ppm}$  over  
286 a range of average culture pH from 7.5 to 8.6 (Figure 5; Table 2). While this is lower by an order of  
287 magnitude than the limited previous studies of boron in sedimentary diatoms (Ishikawa and  
288 Nakamura, 1993), it is similar to boron concentration in the bulk diatom fraction of TC460 (Figure 4D)  
289 and to that observed in previous culturing studies of this diatom species (Figure 5; Meija et al., 2013).  
290 In detail, however, our concentrations are around 2-3 times lower than Meija et al. (2013), perhaps  
291 due to: (i) the different analytical methods used (laser ablation ICP-MS vs. solution here); (ii)  
292 differences in cleaning methods; and/or (iii) differences in culturing methodology. Despite the scatter  
293 between our treatments (also seen in Meija et al., 2013; Figure 5), a least squares regression through  
294 the treatments is significant at the 95% confidence level ( $y = 2.15x - 15.56$ ,  $R^2 = 0.46$ ,  $p = 0.015$ ; Figure  
295 5). The cause of this scatter between treatments is not known but a likely contributor is the relatively  
296 high variability in the carbonate system which was observed in each treatment due to the growth of  
297 the diatoms in this batch culture setup (Figure 2).

298

299 Boron is an essential nutrient for diatoms (Lewin, 1966) and it is likely that boric acid passively diffuses  
300 across the cell wall to ensure the diatom cell has sufficient boron to meet its biological needs.  
301 However, if boric acid were the sole source of boron for the diatoms measured here we might expect  
302 a decrease in boron content as pH increases and external dissolved boric acid concentration declines  
303 (Figure 6).

304

305 Several studies note that a number of higher plants have mechanisms for also actively taking up boron,  
306 leading to large variations in internal boron concentrations (Pfeffer et al., 2001; Dordas and Brown,  
307 2000; Brown et al., 2002). Indeed, on the basis of a similar dataset to that collected here, Meija et al.

308 (2013) suggested that borate is likely transported across the cell wall of *T. weissflogii* as some function  
309 of external borate concentration, which shows a positive relationship with external pH (Figure 6). This  
310 hypothesis is developed and discussed further in the next section.

311

### 312 **3.2.2. Frustule $\delta^{11}\text{B}$ of *T. weissflogii***

313 The  $\delta^{11}\text{B}$  of *T. weissflogii* are isotopically light compared to seawater (39.6 ‰; Foster et al., 2010), with  
314 an average value across all treatments of -3.95 ‰ (Table 2). Despite the scatter between treatments,  
315 similar to the [B] data, Figure 5 shows that there is a clear relationship between the  $\delta^{11}\text{B}$  of the diatom  
316 frustule and pH ( $R^2 = 0.46$ ,  $p < 0.01$ ), albeit with a negative and relatively shallow slope ( $y = -2.61x +$   
317  $17.12$ ).

318

319 These results confirm that biogenic silica, free from clay contamination, has a very light boron isotopic  
320 composition (Ishikawa and Nakamura, 1993). However, the observed relationship between  $\delta^{11}\text{B}$  in *T.*  
321 *weissflogii* and pH is radically different to that which is observed in carbonates (Figure 5), implying a  
322 distinctive incorporation mechanism for boron into diatom opal. Much work has been carried out in  
323 recent years to show that boron is incorporated in carbonates predominantly as the borate ion with  
324 minor, if any, isotopic fractionation (*e.g.* see Branson, 2018 for a review). It is similarly thought that  
325 the borate ion is incorporated into opal in an analogous fashion to its incorporation into clays  
326 (Ishikawa and Nakamura, 1993; Kolodny and Chaussidon, 2004). However, such a mechanism in  
327 isolation would only be able to generate  $\delta^{11}\text{B}$  in opal of  $\sim 13$  ‰ (at the lowest pH). Given the  
328 preponderance of isotopically light diatoms, radiolaria and chert  $\delta^{11}\text{B}$  in the literature (including this  
329 study; Kolodony and Chaussidon, 2004; Ishikawa and Nakamura, 1993), it is therefore likely that there  
330 is an additional light isotopic fractionation of boron on its incorporation into opal, although its  
331 absolute magnitude is currently unknown (Kolodony and Chaussidon, 2004).

332

333 To make their frustules out of biogenic silica, aqueous  $\text{Si}(\text{OH})_4$  is taken up by the diatom cell via active  
334 transport by silicon transporter proteins (Amo and Brzezinski, 1999). Once  $\text{Si}(\text{OH})_4$  has entered the  
335 cell, it accumulates in vacuoles that tend to have a high pH in order to prevent polycondensation of  
336  $\text{Si}(\text{OH})_4$  at its higher concentration in the vacuole (Vrieling et al., 1999). The accumulated  $\text{Si}(\text{OH})_4$  is  
337 then transported to the silicon deposition vesicle (SDV), which is an acidic compartment where the  
338 formation of biogenic silica and the construction of the frustule occurs. Without knowledge of the  
339 isotopic fractionation of boron on incorporation into biogenic silica, the interpretation of our new  $\delta^{11}\text{B}$   
340 data is challenging. This difficulty is further increased given that the fluid in the SDV is unlikely to have  
341 the same  $\delta^{11}\text{B}$  as external seawater and its relatively acidic pH ( $\sim 5.5$ ; Meija et al., 2013; Vrieling et al.,

342 1999) is likely to promote polymerisation of  $\text{Si}(\text{OH})_4$ . Nonetheless, the broad similarity between the  
343  $\delta^{11}\text{B}$  of our cultured *T. weissflogii* with the bulk diatom fraction measured here from sample TC460  
344 and the bulk diatom fraction and radiolarian skeleton measured by Ishikawa and Nakamura (1993; ~3  
345 ‰), suggests that a large part of the light isotopic composition of biogenic silica is driven by the  
346 isotopic fractionation on incorporation rather than “vital effects” relating to the  $\delta^{11}\text{B}$  and pH of the  
347 SDV in the different species and organisms. That being said, the >3‰ range between different pH  
348 treatments in *T. weissflogii* and the >10 ‰ difference between our *Chaetoceros* dominated bulk  
349 diatom fraction from TC460 and the cultured *T. weissflogii*, as well as the negative relationship  
350 between pH and diatom  $\delta^{11}\text{B}$  (Figure 5), argue against a simple two-step model involving borate ion  
351 incorporation from seawater with a fixed isotopic fractionation.

352

353 The  $\delta^{11}\text{B}$  of the fluid from which our *T. weissflogii* precipitated their frustules can be calculated if  
354 we assume the pH in the SDV of our *T. weissflogii* is 5.5 across all our treatments (Mejia et al.,  
355 2013). Given that at this pH the  $\delta^{11}\text{B}$  of borate is ~13 ‰, the isotopic composition of this fluid is  
356 lighter than seawater, even if we assume an arbitrary -10 ‰ isotopic fractionation on  
357 incorporation (blue circles in Figure 7a). Furthermore, the  $\delta^{11}\text{B}$  of the SDV fluid is inversely  
358 correlated with the  $\delta^{11}\text{B}$  of either dissolved borate or dissolved boric acid (Figure 7a).

359 As discussed above and illustrated schematically in Figure 8, Mejia et al. (2013) suggested that  
360 there are two sources of boron in a diatom cell: (i) passively diffused and isotopically heavy boric  
361 acid; and (ii) actively transported isotopically light borate ion (see Figure 8). Assuming that: (a) no  
362 additional fractionation occurs during uptake and diffusion; and (b) only the borate ion is  
363 incorporated into the frustule, we can calculate the relative contribution of these two sources of  
364 boron as a function of external pH (Figure 7b). This treatment shows that the relative  
365 concentration of borate derived boron in the SDV fluid increases as external pH increases, though  
366 the absolute values here are a function of the magnitude of the isotopic fractionation on  
367 incorporation, so we only have confidence in the trends shown in Figure 7b. Nonetheless, given  
368 that the dissolved boric acid concentration decreases and dissolved borate increases as pH is  
369 increased (Figure 6), this is perhaps not surprising.

370 While this finding is entirely compatible with the trend of increasing boron content of *T.*  
371 *weissflogii* observed as pH increases (Figure 5), an added complication is that at pH ~5.5 the  
372 concentration of borate ion in the SDV is likely to be relatively low (Figure 6). However, the  
373 timescales required to reach equilibrium in the boron system are short (e.g. around 95  $\mu\text{s}$ ; Zeebe

374 et al., 2001), meaning that any aqueous borate incorporated into the frustule would be  
375 immediately replenished to its equilibrium value by conversion from the more abundant boric  
376 acid. Although relevant partition coefficients are likely to be different, a similar process ensures  
377 the quantitative removal of boron from pH <7 solutions by the Amberlite 743 anion exchange  
378 resin used for boron purification prior to analysis by MC-ICPMS (see above; Lemarchand et al.,  
379 2002).

380 Active bicarbonate ion uptake accounts for a substantial amount of the carbon fixed by phytoplankton  
381 (e.g. Tortell et al., 2006). As a result, Mejía et al. (2013) proposed that the enrichment of borate ion  
382 into the SDV of *T. weissflogii* and *T. pseudonana* was the result of the active co-transport of borate ion  
383 with bicarbonate ion by bicarbonate transporter proteins. Borate is transported because of its similar  
384 charge and size to  $\text{HCO}_3^-$  and the phylogenetic similarity between bicarbonate and borate transporters  
385 (Mejía et al., 2013). In our model, as external borate ion concentration increases, the borate leak into  
386 the diatom cell is also increased. An additional factor is  $\text{HCO}_3^-$  transport, which may be proportionally  
387 up-regulated as external  $\text{CO}_2$  content decreases (and external pH increases) in order to provide the  
388 diatom cell with sufficient carbon (Mejía et al., 2013). This may therefore offer a way of driving an  
389 elevation of the borate content of the SDV as pH increases (Mejía et al., 2013). Regardless of the exact  
390 mechanism, an SDV fluid with an inverse relationship between  $\delta^{11}\text{B}$  and pH is required to explain the  
391  $\delta^{11}\text{B}$  of the *T. weissflogii* frustule measured here. A simple model whereby external borate ion is an  
392 increasingly important contributor to the boron in the SDV as pH increases is able to explain the  
393 observed dependency of boron content and  $\delta^{11}\text{B}$  on pH. However, a more complete model of the  
394 boron systematics in diatom opal requires a better understanding of isotopic fractionation on  
395 incorporation of boron into biogenic silica, the environmental controls on this fractionation and the  
396 nature of the partitioning of boron within the diatom cell and into biogenic silica.

397

### 398 **3.2.3. Boron-based pH proxies in diatom opal**

399 The  $\delta^{11}\text{B}$ -pH and B-pH relationships derived here for *T. weissflogii* potentially offer two independent  
400 means to reconstruct the past pH of seawater, particularly in those regions key for  $\text{CO}_2$  and heat  
401 exchange where foraminifera are largely absent (e.g. at high latitudes). However, the current  
402 calibrations (Figure 5) are relatively uncertain, which may preclude their application to some  
403 situations. For instance, recasting the  $\delta^{11}\text{B}$ -pH relationship in terms of  $\delta^{11}\text{B}$  as the dependent variable  
404 and using a regression method that accounts for uncertainty in X and Y variables (SIMEX; Carroll et al.,  
405 1996) gives the calculated residual pH of the regression as  $\pm 0.28$  pH units. For the [B] vs. pH  
406 relationship, this uncertainty is  $\pm 0.36$  pH units. At typical surface ocean conditions, such a variability

407 in pH would translate to seawater  $p\text{CO}_2$  variability of up to ca.  $\pm 250$  ppm. Although encouraging, this  
408 treatment suggests that additional work is needed before the relationship between  $\delta^{11}\text{B}$  and boron  
409 content of diatom opal and seawater pH is a sufficiently precise proxy for a fully quantitative past  
410 ocean pH. In particular, future culturing efforts should aim to more carefully control the pH of the  
411 culture media. This could be achieved by either using larger volume dilute batch cultures, by  
412 harvesting the diatoms earlier in the experiment prior to any significant drift in the carbonate system,  
413 and/or by using a more robust steady-state chemostat method (e.g. Leonardos and Geider, 2005).

414

#### 415 **4. Conclusions**

416 In the first study of its kind, we use a modified version of the carbonate boron purification technique  
417 of Foster (2008) to show that the  $\delta^{11}\text{B}$  of *T. weissflogii* opal is pH sensitive but isotopically light (-3.95  
418 ‰ on average) and has an inverse relationship with external seawater pH. Using a novel ICP-MS  
419 method we also show that the boron content of *T. weissflogii* opal increases with increasing pH,  
420 supporting the only other study investigating boron in diatoms (Mejía et al., 2013). This suggests that  
421 more borate is incorporated into the diatom frustule as the dissolved borate abundance increases  
422 with external pH. A simple model is presented, based on Mejía et al. (2013), which implies both of  
423 these findings could be due to there being two distinct sources of the boron in the SDV: external boric  
424 acid and external borate ion, with the balance of each source changing with external pH. While these  
425 results are encouraging, suggesting that the boron proxies in diatom opal may hold considerable  
426 promise as a tracer of past ocean pH, more work is needed to fully understand the boron systematics  
427 of diatom opal. In particular, there is an urgent need to place boron in opal on a firmer grounding with  
428 precipitation experiments in the laboratory at controlled pH to determine the magnitude of boron  
429 isotopic fractionation on boron incorporation into opal as well as the dependence of this fractionation  
430 on other environmental factors.

431

#### 432 **Acknowledgements**

433 We wish to thank Claus-Dieter Hildebrand for supplying the diatom-rich sediment sample TC460. John  
434 Gittins, Mark Stinchcombe, Chris Daniels and Lucie Daniels are acknowledged for their help during the  
435 culturing and subsequent nutrient and carbonate system analysis. Heather Stoll is also thanked for  
436 her useful discussions on this topic. Financial support for this study was provided by the Natural  
437 Environmental Research Council (UK) to H.K.D. (grant number 1362080) and to G.L.F. (NE/J021075/1).

438

#### 439 **Author contribution**

440 GLF, HKD, AJP and CMM conceived and designed the study and it was carried by HKD and NF (aided  
441 by AJP, CMM and GLF). GEAS aided HKD in sample preparation and MPH carried out the carbonate  
442 system measurements of the culture media. GLF and HKD produced the first draft and all authors  
443 contributed to the writing of the study.

444

445 **Competing interests**

446 The authors declare that they have no conflict of interest.

447

448 **Code/Data availability**

449 The data generated in this study is tabulated herein. For any additional data please contact the  
450 corresponding author.

451

452

453

454

455

456

457

458

459 **Figure Captions**

460 **Figure 1.** Diatom growth rate and cell size as a function of pH labelled according to CO<sub>2</sub> treatment.  
461 Linear least squares regressions, including R<sup>2</sup> and p-values are also shown.

462 **Figure 2:** Each culture treatment labelled according to target pCO<sub>2</sub> and showing the evolution in  
463 the culture media through the experiment. All treatments exhibit changes in DIC due to diatom  
464 growth balanced with the input of CO<sub>2</sub>. The higher pCO<sub>2</sub>, the more DIC increases towards the end  
465 of the experiment.

466 **Figure 3:** (a-d) Concentration of Na, Si, Al and B in the Matrix Fraction by ICP-MS. These analyses  
467 suggest blank levels of B are present in the matrix washed off the Amberlite IRA 743 resin-based  
468 column. (e-f) Concentration of the Na, Si and Al in the boron fraction indicating blank levels of Na  
469 (ca. 1.7 ppb) and Si (ca. 1.9 ppb) and a higher concentration of Al (ca. 68 ppb) are present.

470 **Figure 4:** (A) The reproducibility of the TC460 diatom core catcher in-house standard. Samples of  
471 different concentration (~10 to ~30 ng B) lie within error of the mean (5.98 ‰ ± 0.28 ‰, 2σ). This  
472 compares well to carbonates (2σ = 0.20 ‰). (B) Aluminium concentration of the B fraction from  
473 TC460 (as ppb of the solution analysed for δ<sup>11</sup>B) shows no correlation with δ<sup>11</sup>B, likely suggesting  
474 there is no significant effect on mass fractionation for this level of Al. (C) The results of the standard  
475 addition experiment. The blue line is a least squares regression between the measured δ<sup>11</sup>B of each  
476 mixture (green circles) and the calculated δ<sup>11</sup>B of that mixture given known end-member values (end  
477 members shown as blue circles). R<sup>2</sup> = 0.97, p < 0.0001, slope = 1.01 ± 0.07 and intercept = -0.15 ±  
478 0.29. 1:1 line is shown as a black line and dotted blue lines show the 95% confidence limit of the  
479 regression. Note that the end members were not used in the regression. (D) B content in ppm of six  
480 repeat samples of the diatom fraction of TC460. The black line indicates the mean value and the grey  
481 lines show 2σ, of 2.99 ± 0.64 ppm.

482 **Figure 5:** (A) δ<sup>11</sup>B of *T. weissflogii* diatom opal plotted against aqueous borate, labelled according to  
483 pCO<sub>2</sub> treatment. Also shown are published deep sea coral *Desmophyllum dianthus* (Anagnostou et  
484 al., 2012) and foraminifera δ<sup>11</sup>B (*Globigerinoides ruber* and *Orbulina universa*; Henehan et al., 2013;  
485 Henehan et al., 2016, respectively). Least squares regression lines are also shown. Error bars on δ<sup>11</sup>B  
486 borate are shown at 95% level of confidence and relate to the drift in experimental conditions. (B)  
487 *T. weissflogii* opal δ<sup>11</sup>B against pH of each treatment demonstrating a statistically significant negative  
488 relationship. Diatom data is labelled according to pCO<sub>2</sub> treatment. (C) Boron content of cultured *T.*  
489 *weissflogii* diatom opal as a function of pH (using left-axis), labelled according to pCO<sub>2</sub>. A least  
490 squares regression with 95% confidence interval is also shown. In grey (and using the right-hand  
491 axis) are data for *T. weissflogii* from Mejia et al. (2013). Note how both studies show an increase in  
492 boron content with increasing pH, but absolute values differ by a factor of 2-3. Uncertainty in all

493 points is shown at the 95% confidence level. In some cases, the error bars are smaller than the  
494 symbols.

495 **Figure 6:** Plots describing (A) the pH-dependent relationship between the abundance of aqueous  
496 boron species, and (B) the isotopic fractionation observed between boric acid ( $B(OH)_3$ ; red) and  
497 borate ( $B(OH)_4^-$ ; blue) at  $T = 25\text{ }^\circ\text{C}$  and  $S = 35$ .

498 **Figure 7:** (A) Back-calculated  $\delta^{11}\text{B}$  of the silica deposition vesicle (SDV), and (B) the fraction of boron  
499 in the SDV that is derived from external borate. In (A) the diatom  $\delta^{11}\text{B}$  data are shown as grey circles  
500 and the calculated  $\delta^{11}\text{B}$  of the SDV as blue circles. Included in this model is an arbitrary -10 ‰  
501 fractionation between the  $\delta^{11}\text{B}$  of the SDV and the opal precipitated. The fraction of borate in the  
502 SDV in (B) is a function of this assumption so these absolute values should be taken as illustrative  
503 only.

504 **Figure 8.** Schematic of the model described herein for boron uptake by *T. weissflogii*. The speciation  
505 behaviour and isotopic composition of boron is also shown in the insert, with the aqueous species  
506 colour coded (red = boric acid, blue = borate ion). Seawater boric acid diffuses into the diatom cell  
507 and the borate ion is actively transported, with  $\text{HCO}_3^-$ . While it remains unclear how boron enters  
508 the silica deposition vesicle, once inside it respeciates into borate ion and boric acid, with the borate  
509 ion being incorporated into the frustule. The isotopic composition of internal boron is a function of  
510 external pH, which sets the isotopic composition of the incoming species, and the balance between  
511 active borate ion transport and passive boric acid diffusion. The compartments are colour coded  
512 according to approximate pH (scale on the right).

513

514

515



516 **Tables**

517

Treatment	pCO <sub>2</sub> (ppm)	2σ	pH	2σ	DIC (μM)	2σ	HCO <sub>3</sub> <sup>-</sup> (μM)	2σ	Growth rate (d <sup>-1</sup> )
200	125	8	8.53	0.73	1925	61	1091	59	1.03
280	244	73	8.25	0.41	2165	113	1521	260	1.03
400	267	28	8.25	0.44	2400	115	1728	107	0.96
800	809	62	7.83	0.24	2525	56	2206	69	1.01
1600	2117	40	7.48	0.08	2791	21	2628	22	1.01

518 *Table 1: Mean carbonate system parameters experienced under the average growth*  
 519 *conditions as calculated for each culture treatment on the basis of the number of cells*  
 520 *grown in each 24-hour period of the batch experiment.*

521

Treatment	pH (Total scale)	pH 2σ	δ <sup>11</sup> B	δ <sup>11</sup> B 2σ	δ <sup>11</sup> B sw borate	[B] ppm
200	8.55	0.63	-5.51	0.21	24.20	3.15
200	8.54	0.62	-5.40	0.21	24.00	2.81
280	8.27	0.35	-5.05	0.20	20.00	3.72
280	8.18	0.25	-5.66	0.21	18.80	0.93
280	8.30	0.42	-5.79	0.21	20.50	1.04
400	8.26	0.38	-3.64	0.20	19.90	3.37
400	8.24	0.36	-3.57	0.21	19.60	1.26
400	8.25	0.36	-2.41	0.21	19.70	2.68
800	7.85	0.22	-2.93	0.19	15.40	NA
800	7.82	0.18	-2.80	0.22	15.20	0.78
800	7.82	0.20	-3.08	0.21	15.20	1.11
1600	7.48	0.06	-1.94	0.20	13.30	0.74
1600	7.48	0.07	-3.62	0.21	13.30	0.91

522 *Table 2. Treatment name and pH with δ<sup>11</sup>B and [B] for cultured T. weissflogii.*

523

524

525

526

527

528 **References**

- 529 Amo, Y. D., and Brzezinski, M. A.: The chemical form of dissolved Si taken up by marine diatoms,  
530 *Journal of Phycology*, 35, 1162-1170, 10.1046/j.1529-8817.1999.3561162.x, 1999.
- 531 Anagnostou, E., Huang, K.-F., You, C.-F., Sikes, E. L., and Sherrell, R. M.: Evaluation of boron isotope  
532 ratio as a pH proxy in the deep sea coral *Desmophyllum dianthus*: Evidence of physiological pH  
533 adjustment, *Earth Planet. Sci. Lett.*, 349-350, 251-260, 10.1016/j.epsl.2012.07.006, 2012.
- 534 Bradshaw, A. L., Brewer, P. G., Schafer, D. K., and Williams, R. T.: Measurements of total carbon dioxide  
535 and alkalinity by potentiometric titration in the GEOSECS program, *Earth Planet. Sci. Lett.*, 55, 99-115,  
536 doi:10.1016/0012-821X(81)90090-X, 1981.
- 537 Branson, O.: Boron Incorporation into Marine CaCO<sub>3</sub>, in: *Boron Isotopes: The Fifth Element*, edited  
538 by: Marschall, H., and Foster, G., Springer International Publishing, Cham, 71-105, 2018.
- 539 Brown, P. H., Bellaloui, N., Wimmer, M. A., Bassil, E. S., Ruiz, J., Hu, H., Pfeffer, H., Dannel, F., and  
540 Romheld, V.: Boron in plant biology, *Plant Biology*, 4, 205-223, 2002.
- 541 Carroll, R. L., Kuchenhoff, H., Lombard, F., and Stefanski, L. A.: Asymptotics for the SIMEX Estimator in  
542 Nonlinear Measurement Error Models, *Journal of the American Statistical Association*, 91, 242-250,  
543 1996.
- 544 Chalk, T. B., Hain, M. P., Foster, G. L., Rohling, E. J., Sexton, P. F., Badger, M. P. S., Cherry, S. G.,  
545 Hasenfratz, A. P., Haug, G. H., Jaccard, S. L., Martínez-García, A., Pälike, H., Pancost, R. D., and Wilson,  
546 P. A.: Causes of ice age intensification across the Mid-Pleistocene Transition, *Proceedings of the*  
547 *National Academy of Sciences*, 10.1073/pnas.1702143114, 2017.
- 548 Dickson, A. G.: Thermodynamics of the dissociation of boric acid in synthetic seawater from 273.15 to  
549 318.15 K, *Deep Sea Research Part A. Oceanographic Research Papers*, 37, 755-766, doi:10.1016/0198-  
550 0149(90)90004-F, 1990.
- 551 Dickson, A. G., Sabine, C. L. and Christian, J. R., Eds.: SOP 1: Water sampling for the parameters of the  
552 oceanic carbon dioxide system, in *Guide to Best Practices for Ocean CO<sub>2</sub> Measurements*, PICES Special  
553 Publication 3, Chapter 4, North Pacific Marine Science Organization, Sidney, BC, Canada, 2007.
- 554 Dordas, C., and Brown, P. H.: Permeability of boric acid across lipid bilayers and factors affecting it, *J.*  
555 *Membr. Biol.*, 175, 95-105, 2000.
- 556 Foster, G. L.: Seawater pH, pCO<sub>2</sub> and [CO<sub>3</sub><sup>2-</sup>] variations in the Caribbean Sea over the last 130 kyr: A  
557 boron isotope and B/Ca study of planktic foraminifera, *Earth Planet. Sci. Lett.*, 271, 254-266, 2008.

558 Foster, G. L., Pogge von Strandmann, P. A. E., and Rae, J. W. B.: Boron and magnesium isotopic  
559 composition of seawater, *Geochemistry Geophysics Geosystems*, 11, Q08015,  
560 doi:08010.01029/02010GC003201, 2010.

561 Gray, W. R., Rae, J. W. B., Wills, R. C. J., Shevenell, A. E., Taylor, B., Burke, A., Foster, G. L., and Lear, C.  
562 H.: Deglacial upwelling, productivity and CO<sub>2</sub> outgassing in the North Pacific Ocean, *Nature*  
563 *Geoscience*, 11, 340-344, 10.1038/s41561-018-0108-6, 2018.

564 Guerrot, C., Milot, R., Robert, M., and Negrel, P.: Accurate and high-precision determination of boron  
565 isotopic ratios at low concentration by MC-ICP-MS (Neptune), *Geostandards and Geoanalytical*  
566 *Research*, 35, 275-284, 2010.

567 Hasle, G. R., and Fryxell, G. A.: The genus *Thalassiosira*: some species with a linear areola array,  
568 *Proceedings of the Fourth Symposium on Recent and Fossil Marine Diatoms*, Oslo, 1977, 15-66,

569 Hemming, N. G., and Hanson, G. N.: Boron isotopic composition and concentration in modern marine  
570 carbonates, *Geochimica et Cosmochimica Acta*, 56, 537-543, 1992.

571 Hendry, K. R., and Andersen, M. B.: The zinc isotopic composition of siliceous marine sponges:  
572 Investigating nature's sediment traps, *Chem. Geol.*, 354, 33-41, 2013.

573 Henehan, M. J., Rae, J. W. B., Foster, G. L., Erez, J., Prentice, K. C., Kurcera, M., Bostock, H. C., Martinez-  
574 Boti, M. A., Milton, J. A., Wilson, P. A., Marshall, B., and Elliott, T.: Calibration of the boron isotope  
575 proxy in the planktonic foraminifera *Globigerinoides ruber* for use in palaeo-CO<sub>2</sub> reconstruction, *Earth*  
576 *Planet. Sci. Lett.*, 364, 111-122, 10.1016/j.epsl.2012.12.029, 2013.

577 Henehan, M. J., Foster, G. L., Bostock, H. C., Greenop, R., Marshall, B., and Wilson, P. A.: A new boron  
578 isotope-pH calibration for *Orbulina universa*, with implications for understanding and accounting for  
579 vital effects, *Earth Planet. Sci. Lett.*, 454, 282-292, 10.1016/j.epsl.2016.09.024, 2016.

580 Honisch, B., and Hemming, N. G.: Surface ocean pH response to variations in pCO<sub>2</sub> through two full  
581 glacial cycles, *Earth Planet. Sci. Lett.*, 236, 305-314, 2005.

582 Horn, M. G., Robinson, R. S., Rynearson, T., and Sigman, D. M.: Nitrogen isotopic relationship between  
583 diatom-bound and bulk organic matter of cultured polar diatoms, *Paleoceanography*, 26, 1-12, 2011.

584 Ishikawa, T., and Nakamura, E.: Boron isotope systematics of marine sediments, *Earth Planet. Sci. Lett.*,  
585 117, 567-580, 1993.

586 Keller, M. D., Selvin, R. C., Claus, W., and Guillard, R. R. L.: Media for the culture of oceanic  
587 ultraplankton, *Journal of Phycology*, 23, 633-638, 1987.

588 Kolodny, Y., and Chaussidon, M.: Boron isotopes in DSDP cherts: Fractionation and diagenesis, The  
589 Geochemical Society Special Publications, 9, 1-14, 2004.

590 Koning, E., Gehlen, M., Flank, A.-M., Calas, G., and Epping, E.: Rapid post-mortem incorporation of  
591 aluminium in diatom frustules: evidence from chemical and structural analyses, *Mar. Chem.*, 106, 208-  
592 222, 10.1016/j.marchem.2006.06.009, 2007.

593 Lee, K., Kim, T.-W., Byrne, R. H., Millero, F. J., Feely, R. A., and Liu, Y.-M.: The universal ratio of boron  
594 to chlorinity for the North Pacific and North Atlantic oceans, *Geochimica et Cosmochimica Acta*, 74,  
595 1801-1811, doi:10.1016/j.gca.2009.12.027, 2010.

596 Lemarchand, D., Gaillardet, J., Gopel, C., and Manhès, G.: An optimized procedure for boron  
597 separation and mass spectrometry analysis for river samples, *Chem. Geol.*, 182, 323-334, 2002.

598 Leonardos, N., and Geider, R. J.: Elevated atmospheric carbon dioxide increases organic carbon  
599 fixation by *Emiliania huxleyi* (haptophyta), under nutrient-limited high-light conditions, *Journal of*  
600 *Phycology*, 41, 1196-1203, 10.1111/j.1529-8817.2005.00152.x, 2005.

601 Lewin, J.: Boron as a growth requirement for diatoms, *Journal of Phycology*, 2, 160-163,  
602 10.1111/j.1529-8817.1966.tb04616.x, 1966.

603 Lueker, T. J., Dickson, A. G., and Keeling, C. D.: Ocean  $p\text{CO}_2$  calculated from dissolved inorganic carbon,  
604 alkalinity, and equations for K1 and K2: validation based on laboratory measurements of  $\text{CO}_2$  gas and  
605 seawater at equilibrium *Mar. Chem.*, 70, 105-119, doi:10.1016/S0304-4203(00)00022-0, 2000.

606 Martin, J.: Glacial-interglacial  $\text{CO}_2$  change: The iron hypothesis, *Paleoceanography*, 5, 1-13, 1990.

607 Martinez-Boti, M. A., Marino, G., Foster, G. L., Ziveri, P., Hennehan, M. J., Rae, J. W. B., Mortyn, P. G.,  
608 and Vance, D.: Boron isotope evidence for oceanic carbon dioxide leakage during the last deglaciation,  
609 *Nature*, 518, 219-222, 10.1038/nature14155, 2015.

610 Mejia, L. M., Isensee, K., Menendez-Vicente, A., Pisonero, J., Shimizu, N., Gonzalez, C., Monteleone, B.  
611 D., and Stoll, H.: B content and Si/C ratios from cultured diatoms (*Thalassiosira pseudonana* and  
612 *Thalassiosira weissflogii*): Relationship to seawater pH and diatom carbon acquisition, *Geochimica et*  
613 *Cosmochimica Acta*, 123, 322-337, 10.1016/j.gca.2013.06.011, 2013.

614 Ni, Y., Foster, G. L., and Elliott, T.: The accuracy of  $\delta^{11}\text{B}$  measurements of foraminifers, *Chem. Geol.*,  
615 274, 187-195, 2010.

616 Pearson, P. N., and Palmer, M. R.: Atmospheric carbon dioxide concentrations over the past 60 million  
617 years, *Nature*, 406, 695 - 699, 2000.

618 Pfeffer, H., Daniel, F., and Romheld, V.: Boron compartmentation in roots of sunflower plants of  
619 different boron status: A study using the stable isotopes  $^{10}\text{B}$  and  $^{11}\text{B}$  adopting two independent  
620 approaches *Physiol. Plant.*, 113, 346-351, 2001.

621 Rae, J. W. B., Foster, G. L., Schmidt, D. N., and Elliott, T.: Boron isotopes and B/Ca in benthic  
622 foraminifera: proxies for the deep ocean carbonate system, *Earth Planet. Sci. Lett.*, 302, 403-413,  
623 2011..

624 R Core Team (2018). R: A language and environment for statistical computing. R Foundation for  
625 Statistical Computing, Vienna, Austria. URL <https://www.R-project.org/>.

626 Sigman, D. M., and Boyle, E. A.: Glacial/Interglacial variations in atmospheric carbon dioxide, *Nature*,  
627 407, 859-869, 2000.

628 Sigman, D. M., Hain, M. P., and Haug, G. H.: The polar ocean and glacial cycles in atmospheric  $\text{CO}_2$   
629 concentration, *Nature*, 466, 47-55, doi:10.1038/nature09149, 2010.

630 Sosdian, S. M., Greenop, R., Hain, M. P., Foster, G. L., Pearson, P. N., and Lear, C. H.: Constraining the  
631 evolution of Neogene ocean carbonate chemistry using the boron isotope pH proxy, *Earth Planet. Sci.*  
632 *Lett.*, 248, 362-376, doi:10.1016/j.epsl.2018.06.017, 2018.

633 Swann, G. E. A., Pike, J., Snelling, A. M., Leng, M. J., and Williams, M. C.: Seasonally resolved diatom  
634  $\delta^{18}\text{O}$  records from the West Antarctic Peninsula over the last deglaciation, *Earth Planet. Sci. Lett.*, 364,  
635 12-23, 10.1016/j.epsl.2012.12.016, 2013.

636 Tipper, E. T., Galy, A., and Bickle, M.: Calcium and magnesium isotope systematics in rivers draining  
637 the Himalaya-Tibetan-Plateau region: Lithological or fractionation control?, *Geochimica et*  
638 *Cosmochimica Acta*, 72, 1057-1075, 2008.

639 Tortell, P. D., Martin, C. L., and Corkum, M. E.: Inorganic carbon uptake and intracellular assimilation  
640 by subarctic Pacific phytoplankton assemblages, *Limnology and Oceanography*, 51, 2102-2110,  
641 10.4319/lo.2006.51.5.2102, 2006.

642 van Heuven, S., Pierrot, D., Rae, J. W. B., Lewis, E., and Wallace, D. W. R.: MATLAB Program Developed  
643 for  $\text{CO}_2$  System Calculations, doi:10.3334/CDIAC/otg.CO2SYS\_MATLAB\_v1.1, 2011.

644 Vogl, J., and Rosner, M.: Production and certification of a unique set of isotope and delta reference  
645 materials for boron isotope determination in geochemical, environmental and industrial materials,  
646 *Geostandards and Geoanalytical Research*, 36, 161-175, 2012.

- 647 Vrieling, E. G., Gieskes, W. W. C., and Beelen, T. P. M.: Silicon deposition in diatoms: control by pH  
648 inside the silicon deposition vesicle, *Journal of Phycology*, 35, 548-559, 10.1046/j.1529-  
649 8817.1999.3530548.x, 1999.
- 650 Zeebe, R. E., Sanyal, A., Ortiz, J. D., and Wolf-Gladrow, D. A.: A theoretical study of the kinetics of the  
651 boric acid-borate equilibrium in seawater, *Mar. Chem.*, 73, 113-124, 2001.

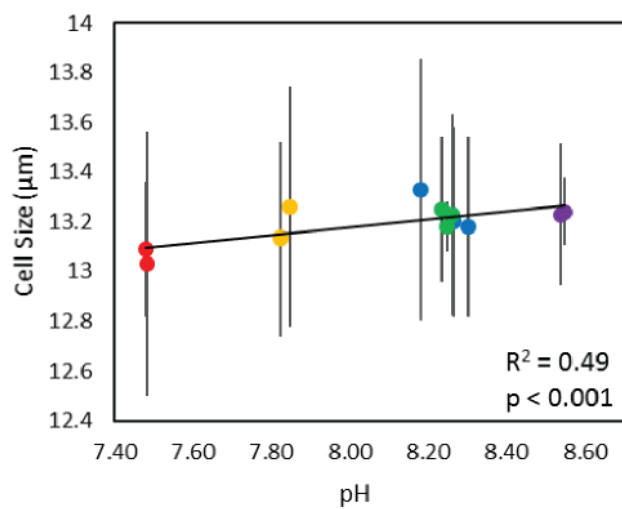
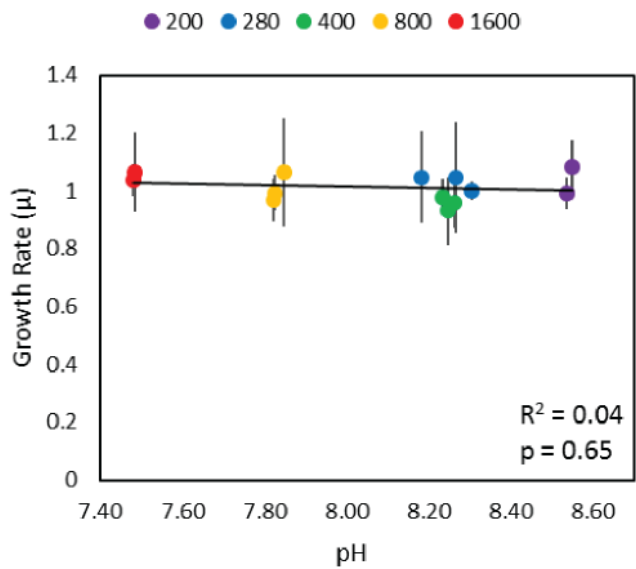


**Figure 1**

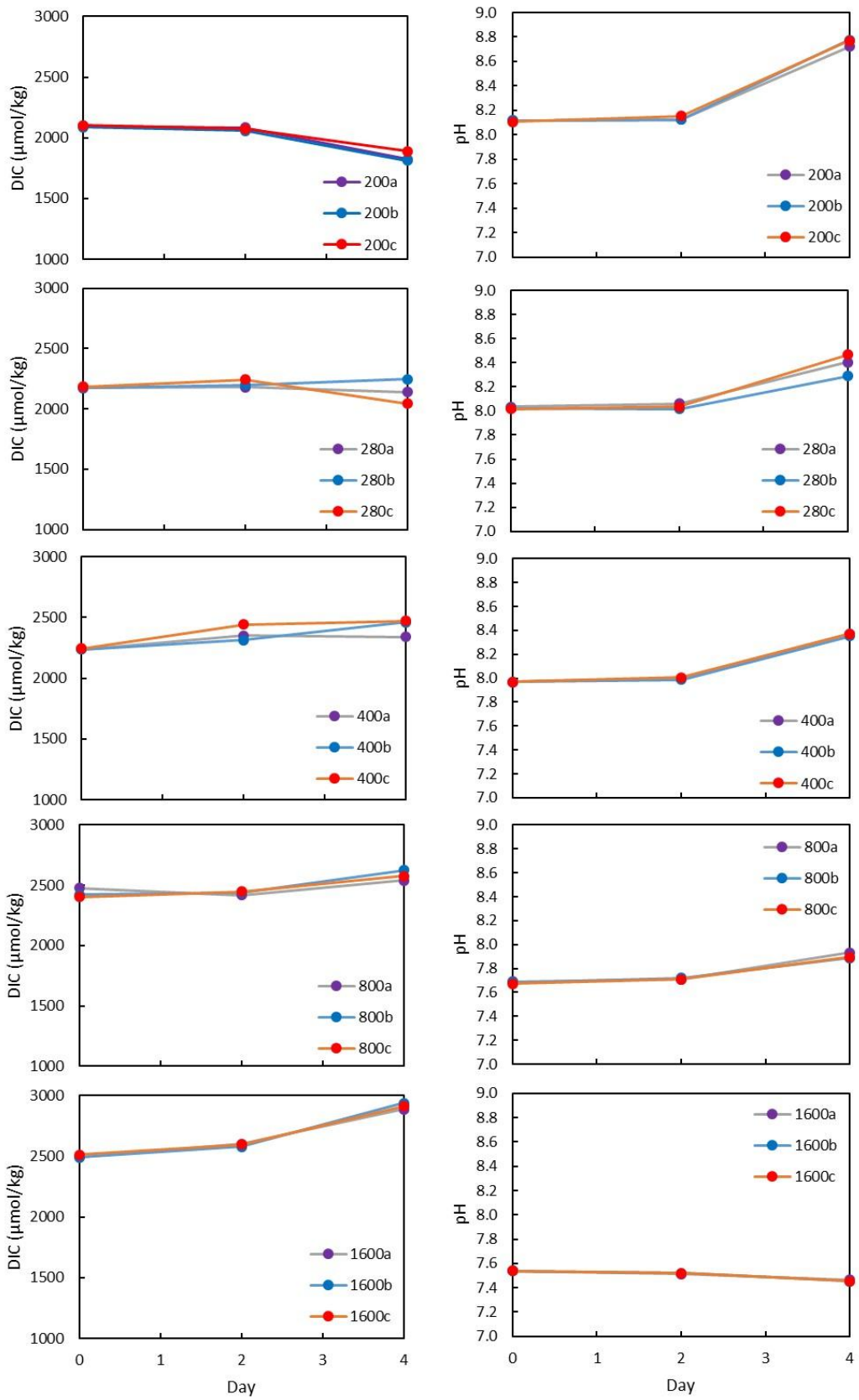


Figure 2



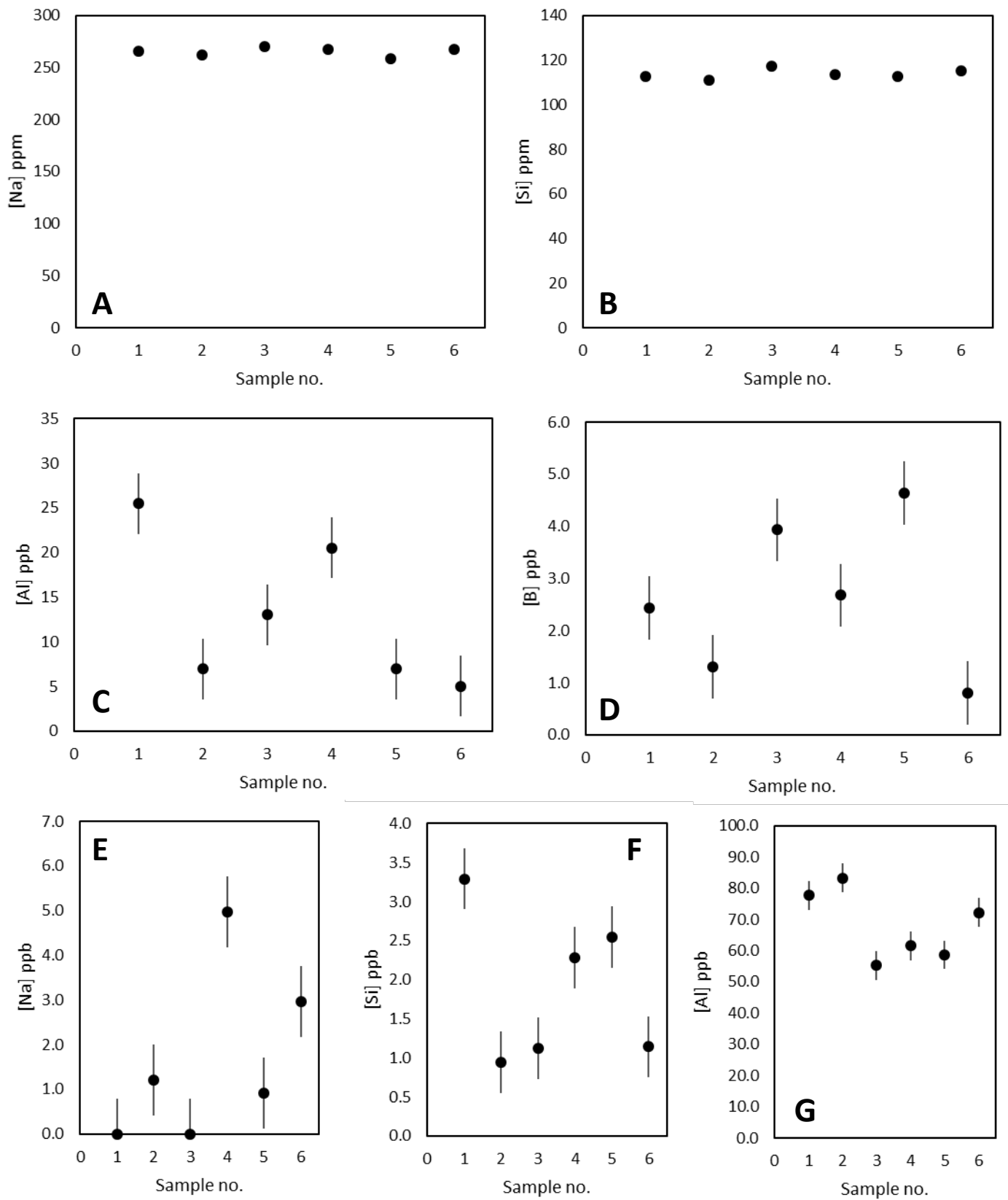


Figure 3.

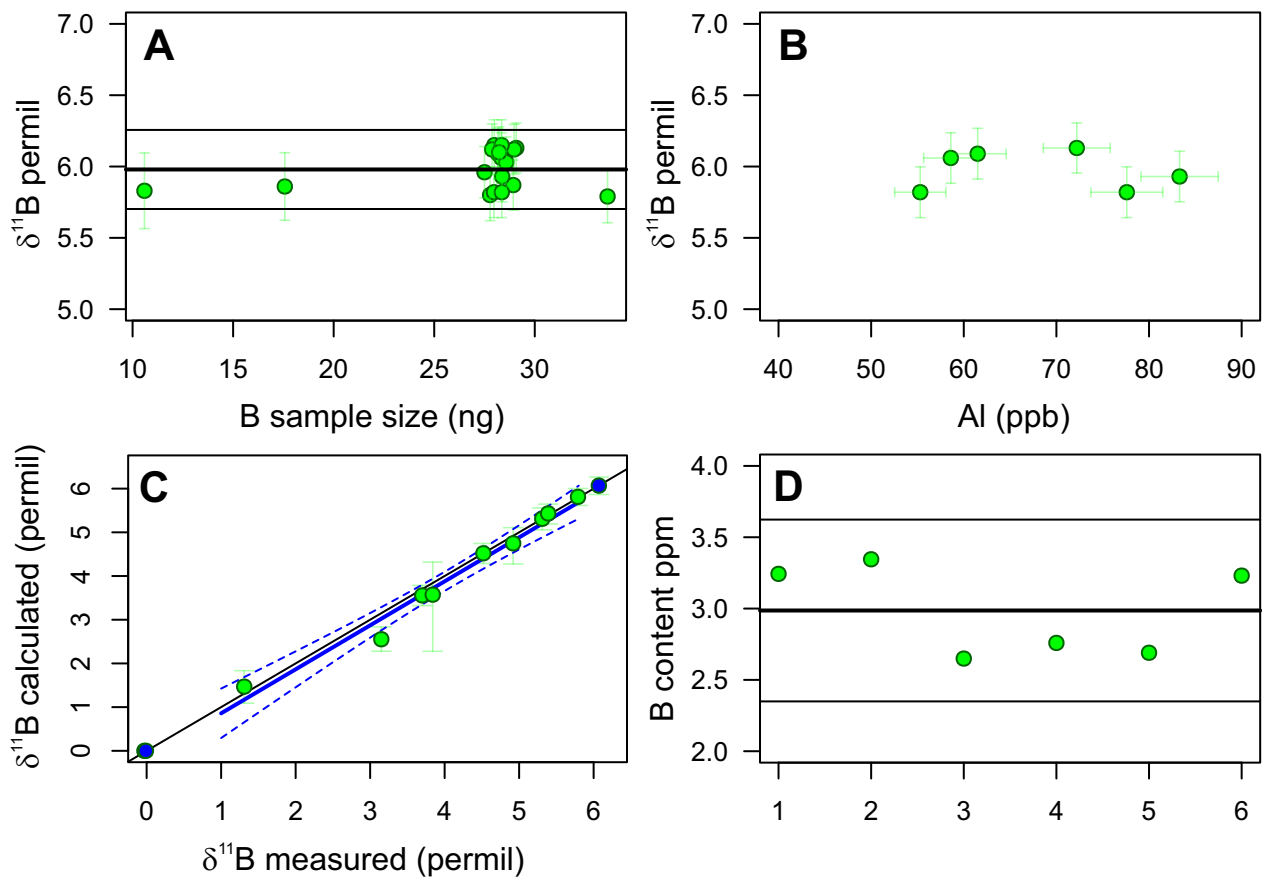


Figure 4

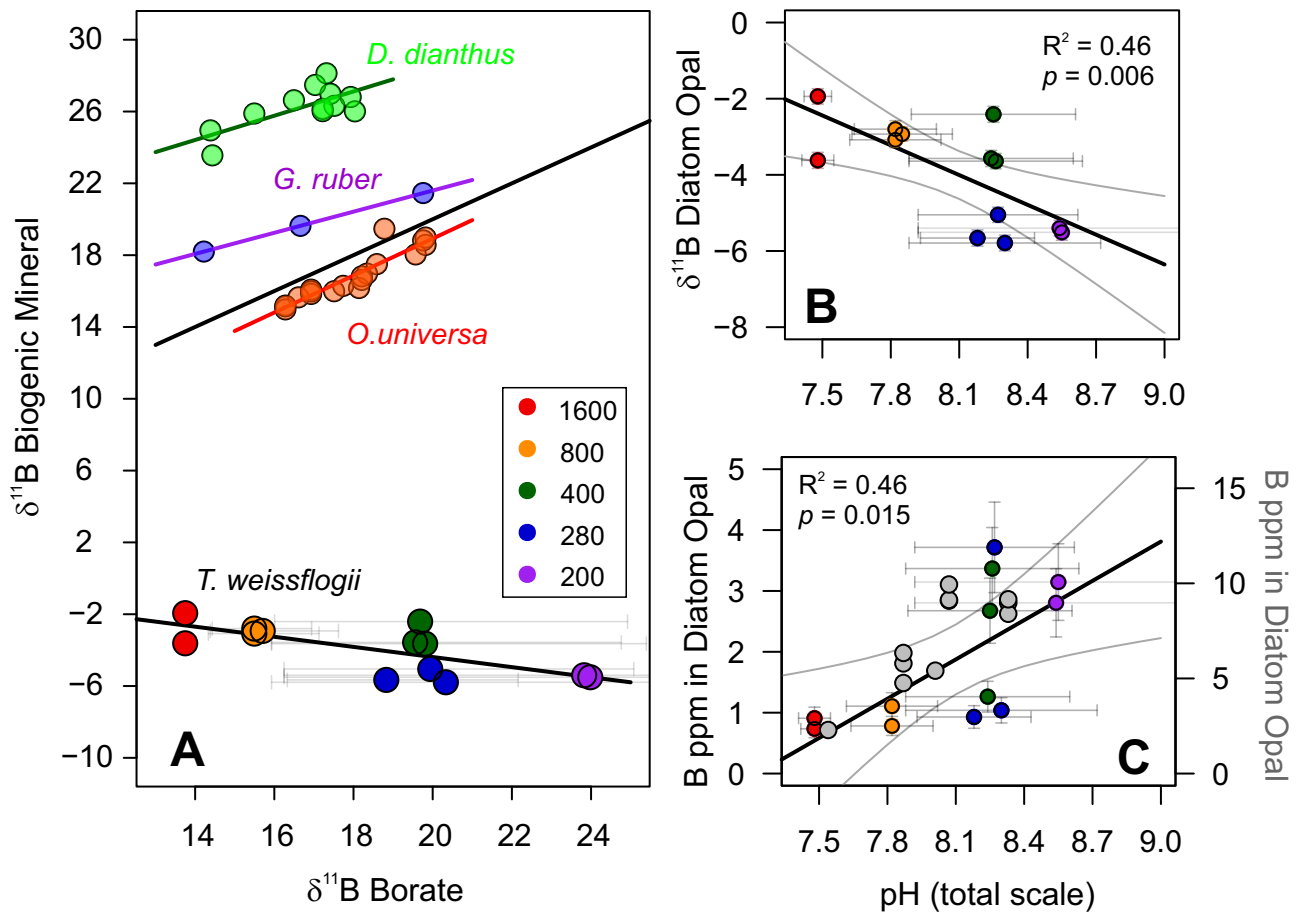


Figure 5

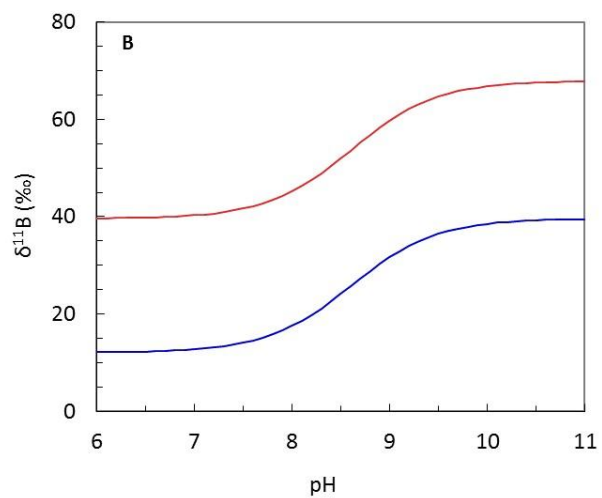
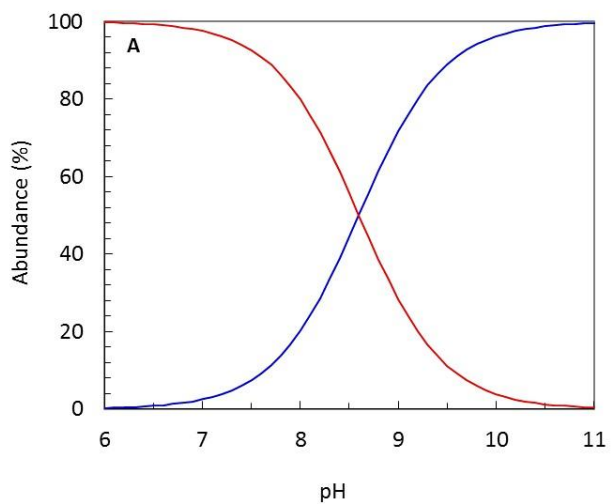


Figure 6.

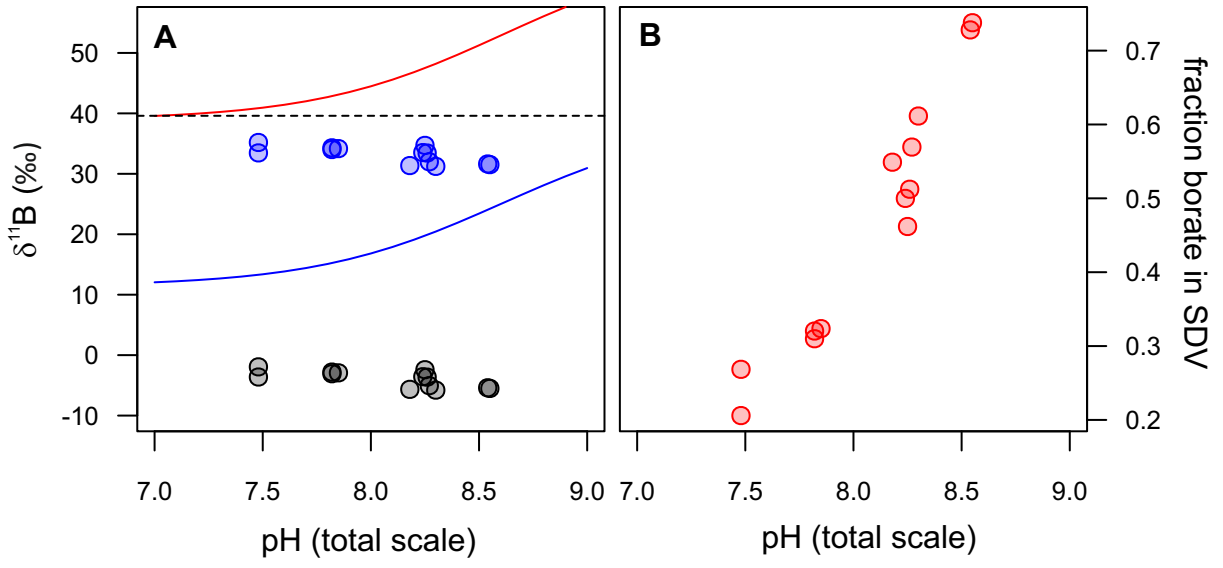


Figure 7

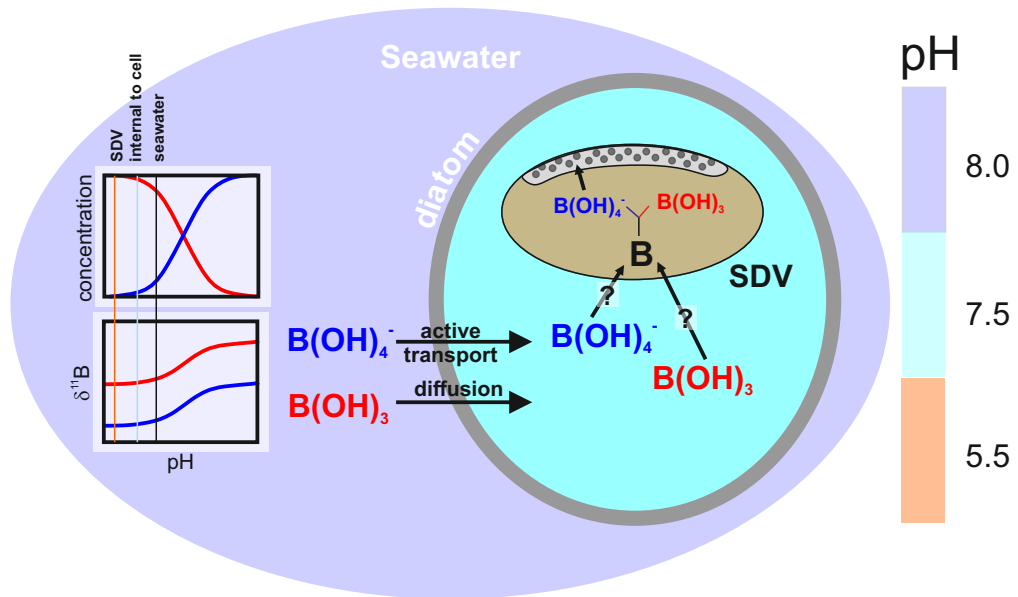


Figure 8.